Received: 17 April 2019 | Revised: 20 May 2019 | Accepted: 21 May 2019

DOI: 10.1002/est2.73

RESEARCH ARTICLE

ENERGY STORAGE WILEY

Few-layer graphene coated on indium tin oxide electrodes prepared by chemical vapor deposition and their enhanced glucose electrooxidation activity

Aykut Caglar[1] | **Berdan Ulas**[1] | **Ozlem Sahin**[2] | **Hilal Demir Kivrak**[1]

[1]Faculty of Engineering, Department of Chemical Engineering, Van Yuzuncu Yil University, Van, Turkey

[2]Faculty of Engineering, Department of Chemical Engineering, Konya Technical University, Konya, Turkey

Correspondence
Hilal Demir Kivrak, Faculty of Engineering, Department of Chemical Engineering, Van Yuzuncu Yil University, Van 65000, Turkey.
Email: hilalkivrak@gmail.com, hilalkivrak@yyu.edu.tr

Funding information
The Scientific and Technological Research Council of Turkey (TUBITAK), Grant/Award Number: 116M004

ABSTRACT

At present, few-layer graphene is deposited on copper (Cu) foil by chemical vapor deposition (CVD) method. Then, the few-layer graphenes produced on the Cu foil are coated onto the indium tin oxide (ITO) electrode to investigate their glucose electrooxidation activities. Hexane and hydrogen flow rate and deposition time parameters with CVD method are examined on different Cu foils. These electrodes are characterized by scanning electron microscopy-energy dispersive X-ray analysis (SEM-EDX), X-ray photoelectron spectroscopy (XPS), and Raman spectroscopy. Furthermore, glucose electrooxidation is examined with cyclic voltammetry (CV), chronoamperometry (CA), and electrochemical impedance spectroscopy (EIS) measurements. One could note that the graphene network is clearly visible from SEM images. The deconvoluted XPS spectrum indicates that carbon appeared in the form of non-oxygenated ring C atoms for few-layer graphene. The few-layer graphene structure is confirmed by Raman analysis. Few-layer graphene/ITO produced at 5 sccm Hexane and 50 sccm hydrogen flow rate and 20 minutes deposition time (G7/ITO) reveals the best electrode activity. The specific activity of G7/ITO electrode is obtained as 6.58 mA cm^{-2}. According to CV, CA, and EIS results, G7/ITO electrode has high electrocatalytic activity, stability, and resistance in comparison with other electrodes.

KEYWORDS
chemical vapor deposition, glucose electrooxidation, graphene, indium tin oxide

1 | INTRODUCTION

Energy is one of the most important requirements for human life. However, the energy need is currently increasing due to the growth in world population and industry. Therefore, alternative energy sources are investigated to meet the energy needs.[1-4] Recently, research studies have been concentrated on fuel cells as alternative energy devices. Fuel cells are clean, efficient, and promising technology for the future.[5] Fuel cells are available of different types such as proton exchange membrane fuel cells,[6-8] direct methanol fuel cells,[9-11] direct ethanol fuel cells,[12,13] alkaline fuel cells,[14] direct formic acid fuel cells,[15] direct urea fuel cells,[16] direct ethylene glycol fuel cells,[17] and direct glucose fuel cells.[18] Glucose is the valuable carbohydrate in nature and could be readily extracted from biomass. Glucose

electrooxidation (GOR) has been carried out to provide an electrochemical glucose sensor for the quick, reliable treatment, and control of diabetes. Furthermore, implantable enzymatic glucose fuel cells used for artificial organs have been the subject of research.[19] Hence, glucose is researched for alternative energy sources as a fuel. Glucose could be directly oxidized to produce electricity but the detection of glucose is classified into two types as (a) enzymatic and (b) nonenzymatic glucose detection.[20-23] Although, enzyme-based GOR has advantages such as high sensitivity and low response time, low chemical stability, and complex synthesis are disadvantages of GOR. Therefore, nonenzymatic GOR has been investigated to prevent deficiencies arising from enzymatic GOR in literature.[21,24] According to these literature studies, the glucose-fed alkaline membrane fuel cells exhibit better activity than the proton conducting membrane fuel cells.[25] When the glucose is fed with an alkaline membrane, 24 electrons are produced for the complete oxidation of CO_2 given as follows:

Glucose	Anode	$C_6H_{12}O_6 + 24OH^- \rightarrow 6CO_2 + 12H_2O + 24e^-$
	Cathode	$12H_2O + 24e^- + 6O_2 \rightarrow 24OH^-$
	Overall	$C_6H_{12}O_6 + 6O_2 \rightarrow 6CO_2 + 6H_2O$

Glucose could be employed as a fuel in fuel cells and it is directly oxidized to produce electricity such as other alcohol fuel cells.[26,27] Current density and potential range values on various catalysts for GOR compiled from literature are given in Table 1. As shown in Table 1, few-layer graphene has not been employed as anode material for GOR in literature. While preparing few layer graphene by chemical vapor deposition (CVD), the surface defects of few layer could be controlled. Our aim is to obtain a relation between GOR and surface defects of few layer graphene leading to explanation of structure sensitivity. In this study, few-layer graphene was coated on Cu foil by CVD method and then was covered on ITO surface. Electrochemical measurements of the graphene/ITO electrodes were obtained on GOR.

Graphene has a hexagonal, single-atom, and two-dimensional (2D) sp^2-hybrid carbon atom layer separated from 3D structured graphite. However, the graphene is known as the first two-dimensional structure in the world. Recently, it has been recognized as one of the most sought-after 2D layered nanomaterial with its superior performance and potential application.[33-36] Graphene production techniques have been known mechanical cleavage, chemical peeling, epitaxial growth, Hummers method, sublimation of 4H—SiC, electrochemical reduction, and CVD.[37-40] Among these methods, CVD is layer system formed on the surface of a solid material and it is a short-time and simple method.[40-42]

Vaporous carrier gas exposes to the surface of a material via heating in a closed container, mostly used in graphene synthesis. CVD is one of the best methods in the production of graphene in a wide range of structures and diameters.[43] Wimalananda et al[44] and Murdock et al[45] reported large-area graphene synthesis on Cu foil with different purity by CVD method. Kong et al[46] reported the single-walled carbon nanotube synthesis by the CVD method of hexane decomposition at elevated temperatures. The precursors containing carbon or its species (such as hexane) are carrier gases used for graphene synthesis by the CVD method. Although, many substrates are used in this method, Cu foil is easy to find, compatible with process and cheap.[45,47]

Surface electronic properties to obtain highly active anode materials are crucial for GOR. Our aim is to modify surface electronic properties of few layer graphene to

TABLE 1 Studies in the literature related to GOR

Catalysts	Preparation method	Solution (glucose) (M)	Potential range (V)	Current (mA/cm^2)	References
Pd_3Sn_2/C	A modified microwave-assisted polyol	0.5	−0.7~0.5	3.64	25
PdRh/C	A modified pulse microwave assisted polyol	0.5	−0.7~0.5	3.50	26
Au/MnO_2—C	$NaBH_4$ reduction	0.5	−1~0.6	2.50	27
$Pd_{30}Au_{70}$/C	A modified pulse microwave assisted polyol	0.05	−1~0.5	3.00	19
Au/C	A water-in-oil microemulsion	0.1	0.1~1.2	2.58	28
Pd/C	A water-in-oil microemulsion	0.1	0.1~1.2	0.92	28
Ni_4Co_2/AC	$NaBH_4$ reduction	1	0~0.8	2.84	29
Pd—Bi/C (1:0.25)	A one-pot polyol	0.02	−0.8~0.5	12.90	30
Pd/CeO_2—C-3	A pulse microwave assisted polyol	0.02	−0.8~0.4	~5.60	31
PtPdAu/C	$NaBH_4$ reduction	0.05	−1~0.6	3.40	32

Abbreviation: GOR, glucose electrooxidation.

enhance GOR activity. Hence, synthesis conditions were optimized to obtain optimum surface property for GOR. The few-layer graphene was coated on Cu foil by the CVD method at varying hexane and hydrogen flow rate and deposition time parameters. Few layer graphene on Cu foil was transferred to ITO electrode surface. ITO electrode was used as working electrode for electrochemical measurements in three electrode system. The few-layer graphene on the Cu foils were characterized by surface analytical technique, such as scanning electron microscopy-energy dispersive X-ray analysis (SEM-EDX), X-ray photoelectron spectroscopy (XPS), and Raman spectroscopy measurements. To investigate their GOR activities, CV, CA, and EIS electrochemical measurements were used.

2 | EXPERIMENTAL

2.1 | Few-layer graphene production by CVD method on Cu foil

Graphene layer on Cu foil was obtained with CVD system. Cu foil was first cleaned by acetone, isopropyl alcohol (IPA), and placed on the substrate holder. Cu films were annealed at 900°C to 1000°C to increase grain size under Ar/H_2 atmosphere. Hydrogen was then fed into the reactor. After the hydrogen gas was cleaned the reactor medium for a time, the reactor was set to 950°C without interrupting the flow. The temperature was increased by 50°C/min. The desired temperature was reached for a total of 19 minutes. When the temperature reaches the desired level, firstly, Cu foil was exposed to hydrogen gas. Then, the hexane was fed to the reactor medium and its flow rate was fixed at 0.5 to 7.5 sccm. After 20 to 40 minutes, the gas flows were cut off and the reactor temperature was brought to room temperature. In this study, several parameters such as hexane flow rate, hydrogen flow rate, and deposition time were investigated through the synthesis of few-layer graphene. Few-layer graphene synthesis conditions are given in Table 2.

TABLE 2 Conditions of few-layer graphene synthesis by CVD method

Run no.	Hexane flow rate (sccm)	Hydrogen flow rate (sccm)	Time (min)	Temperature (°C)
G1	0.5	5	40	950
G2	0.5	5	20	950
G3	0.5	0	40	950
G4	2.5	25	40	950
G5	2.5	25	20	950
G6	2.5	0	40	950
G7	5	50	20	950
G8	7.5	0	40	950
G9	5	0	40	950

Abbreviation: CVD, chemical vapor deposition.

FIGURE 1 Few-layer graphene coated Cu foil

2.2 | Few-layer graphene transfer to the ITO surface

Graphene production process was terminated by the CVD process. Then, polymethylmethacrylate (PMMA) was used to transfer graphene to the ITO surface. The protective polymer layer PMMA was coated on the graphene surface. First, calculated amount of PMMA in powder form was weighed and added to glass bottle containing 10 mL chloroform. The graphene coated Cu foil was placed on the turntable. Then, 0.3 mL of PMMA solution was added onto the few-layer graphene and the coating was started. The coating condition was performed at 500 to 3000 rpm during 5 to 30 seconds. After this process, the sample was taken on the plate and heated at 90°C for 2 minutes to completely dry on the graphene surface.

Iron (III) chloride solution was prepared in a flask. This solution was taken into a petri dish. The graphene coated Cu foil was floated on the top of solution. After a while, it was seen that the Cu layer began to dissolve as shown in Figure 1. For a while, Cu layer resolved completely.

PMMA coated graphene was taken into pure water to remove impurities from iron (III) chloride. The transferred PMMA-coated few-layer graphene was transferred onto the desired substrate. In this study, ITO coated glass substrate was used. After PMMA-coated few-layer graphene transferred over distilled water, it was dried on ITO-coated glass substrate for 15 minutes at 60°C. Few-layer graphene was obtained by dissolving the surface PMMA layer with acetone.

2.3 | Characterization measurements

Few-layer graphene/Cu foils were characterized by SEM-EDX, XPS, and Raman spectroscopy. SEM-EDX was analyzed using

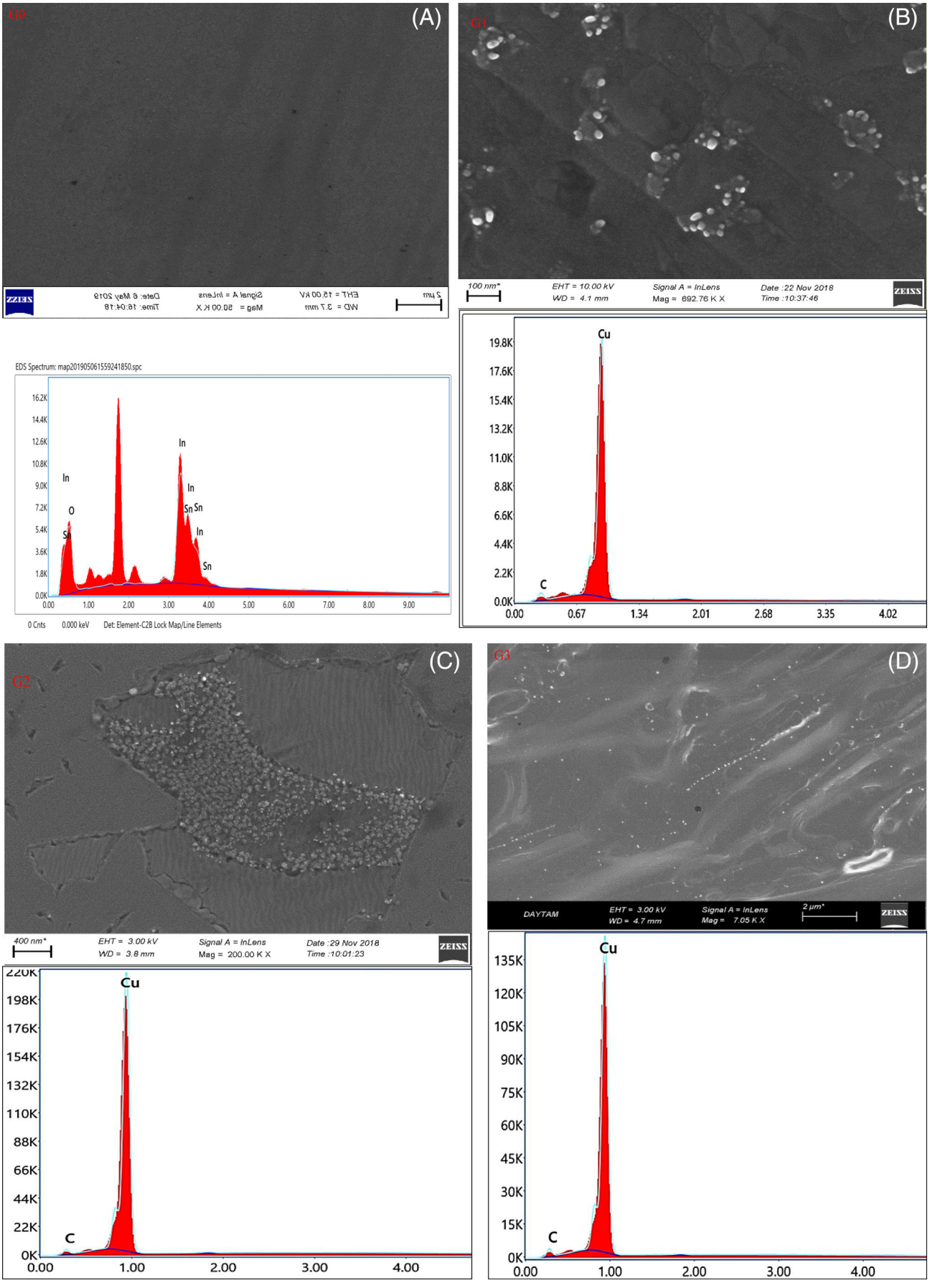

FIGURE 2 SEM images of the samples and corresponding EDX plots. EDX, energy dispersive X-ray analysis; SEM, scanning electron microscopy

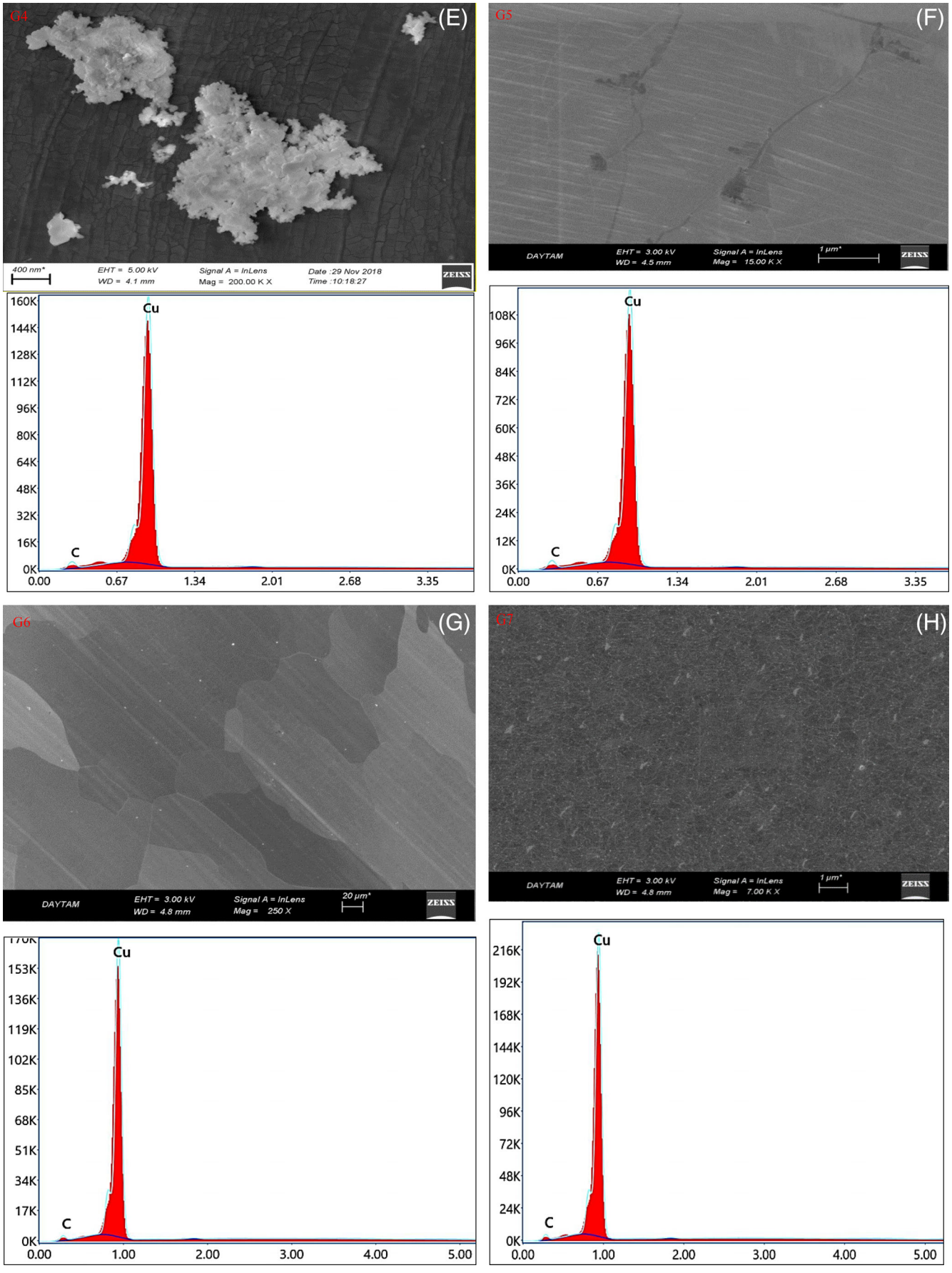

FIGURE 2 (Continued)

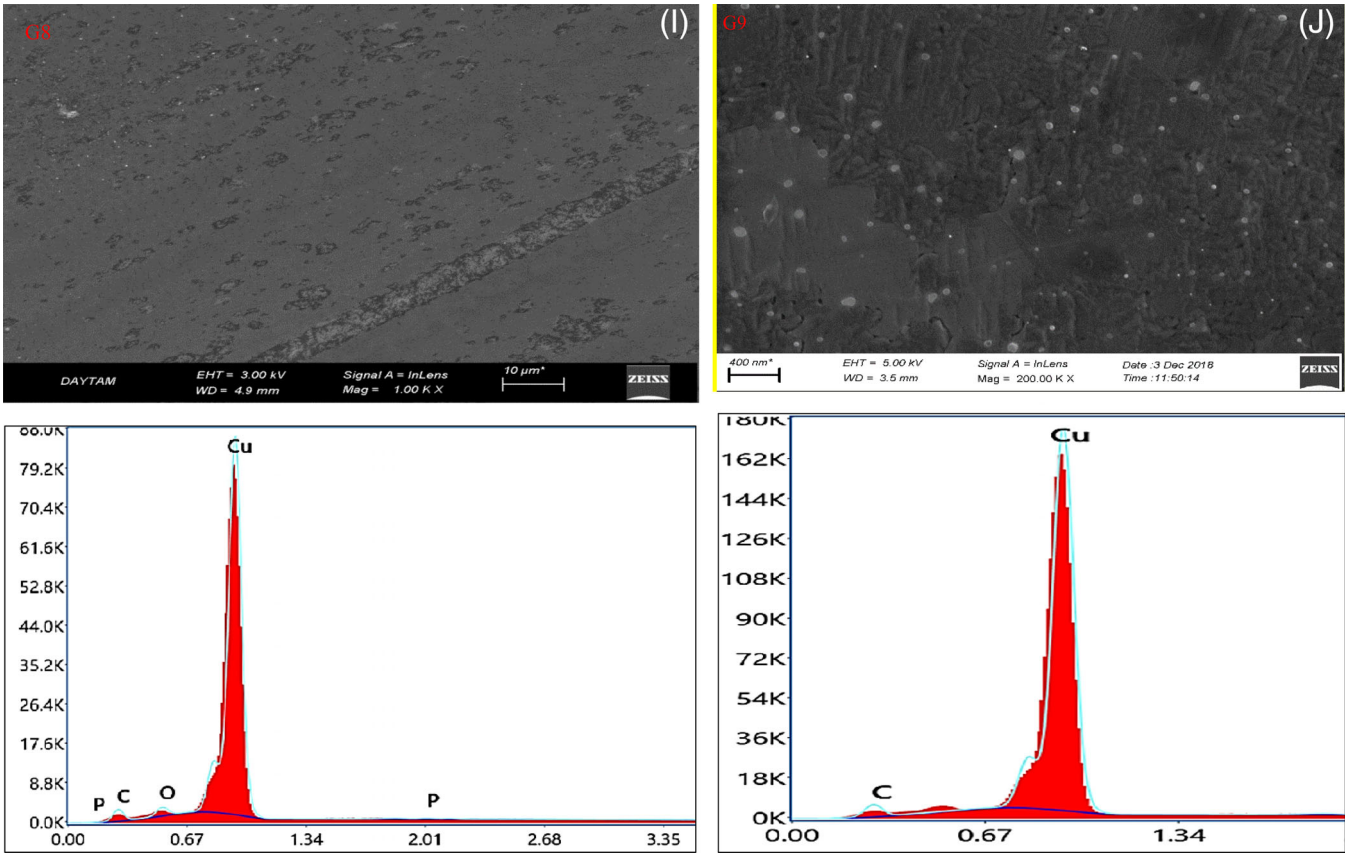

FIGURE 2 (Continued)

the ZEISS SIGMA 300 to scan the surface of few-layer graphene. XPS analysis was performed by Specs-Flex instrument to determine the oxidation state of the few-layer graphene. Raman spectroscopy measurements of these electrodes were obtained by employing Raman Scope II to determine intermolecular vibration energy.

2.4 | Electrochemical measurements of few-layer graphene/ITO electrodes

All electrooxidation measurements were investigated to determine the GOR activities of few-layer graphene/ITO electrodes with CV, CA, and EIS in 1 M KOH + 0.5 M glucose solution. These measurements were obtained using the CHI 660E potentiostat with three electrode systems. The area of the working electrode was 0.44 cm^2. CV measurements were taken at a scan rate of 50 mV s^{-1} at −0.6~0.4 potential range in 1 M KOH + 0.5 M glucose solution. In order to measure the stability of the few-layer graphene/ITO electrodes, 1000 seconds and −0.5 V were examined via CA. The electrochemical resistance of few-layer graphene/ITO electrodes was measured with EIS at 320 kHz and 0.05 Hz to 0.005 V amplitude.

3 | RESULTS AND DISCUSSION

3.1 | Characterization

Figure 2 shows the few layer graphene formation on Cu foils at varying and corresponding EDX plot. G0 represents the graphene free electrode and its EDX spectrum consists of In, Sn, and oxygen. The multi-layer graphene network was clearly seen from Figure 2B-I. It could be seen from Figure 2 that Cu grains were observed clearly. Figure 2B-E and G-I, it was demonstrated the existence of inhomogeneous dark flakes and graphene wrinkles. The observation of graphene wrinkles was attributed to the difference of thermal expansion coefficient between Cu and graphene.[48] The elemental composition of the samples was confirmed by using SEM-EDX, and the results were presented in Table 3. The carbon content for all samples ranges between 12% and 20%. All samples except G8 contain only C and Cu while G8 contains 4.43% oxygen and 0.49% phosphorus.

The XPS spectra of G1, G3, G4, G7, and G9 are displayed in Figures 3 and 4. All XPS spectra were deconvulated by Origin 7.5 and normalized in according to C1s peak (284.6 eV). It was observed that carbon existed in form of C—C, C—O, and O—C═O at binding energy of

TABLE 3 Atomic elemental composition of the samples

Elements (%)	Samples									
	G0	G1	G2	G3	G4	G5	G6	G7	G8	G9
C	0	18.53	12.29	17.77	16.37	18.27	11.38	17.79	17.51	19.96
Cu	0	81.47	87.71	82.23	83.63	81.73	88.62	82.21	77.56	80.04

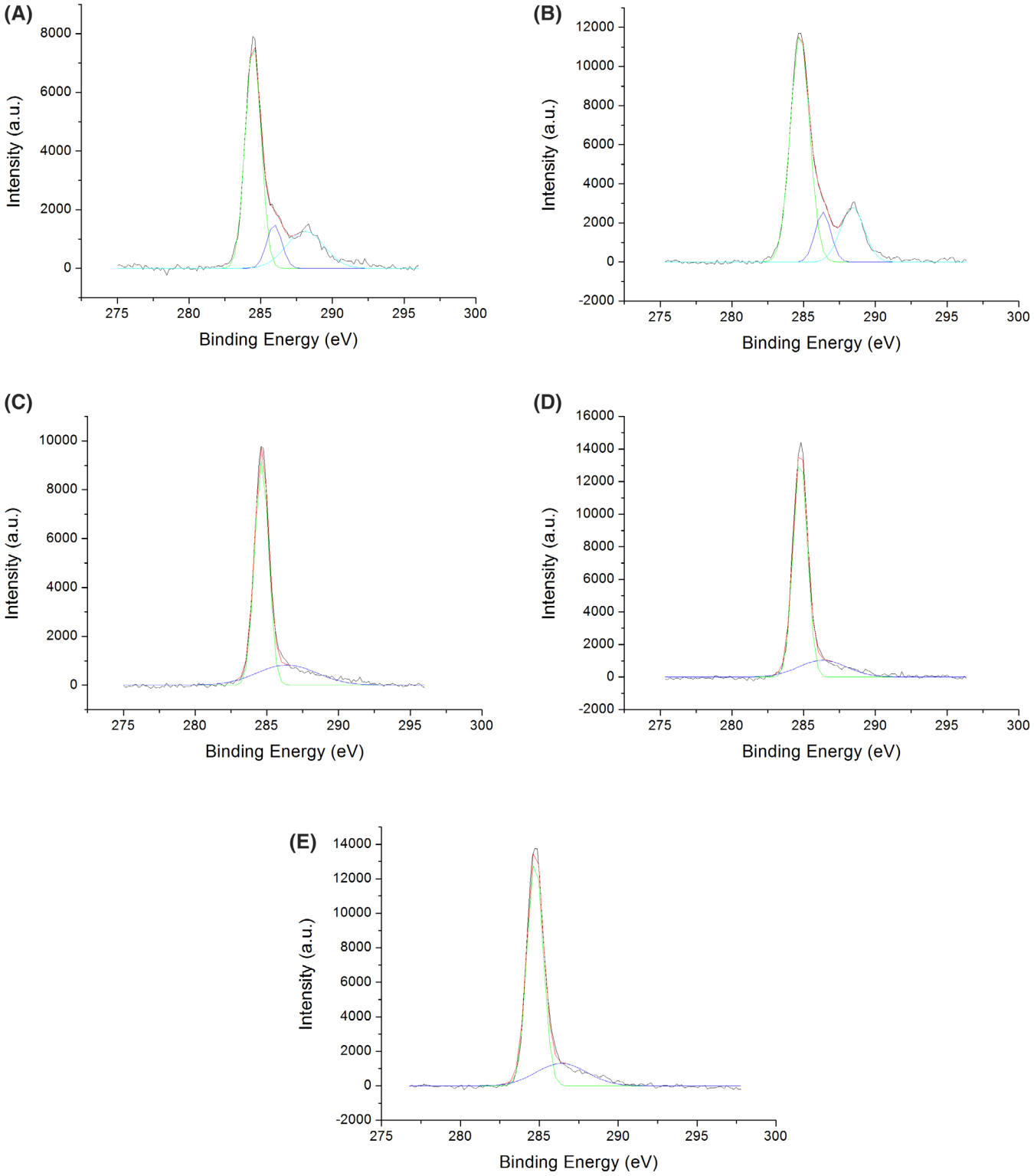

FIGURE 3 C1s spectra of A, G1; B, G3; C, G4; D, G7; and E, G9

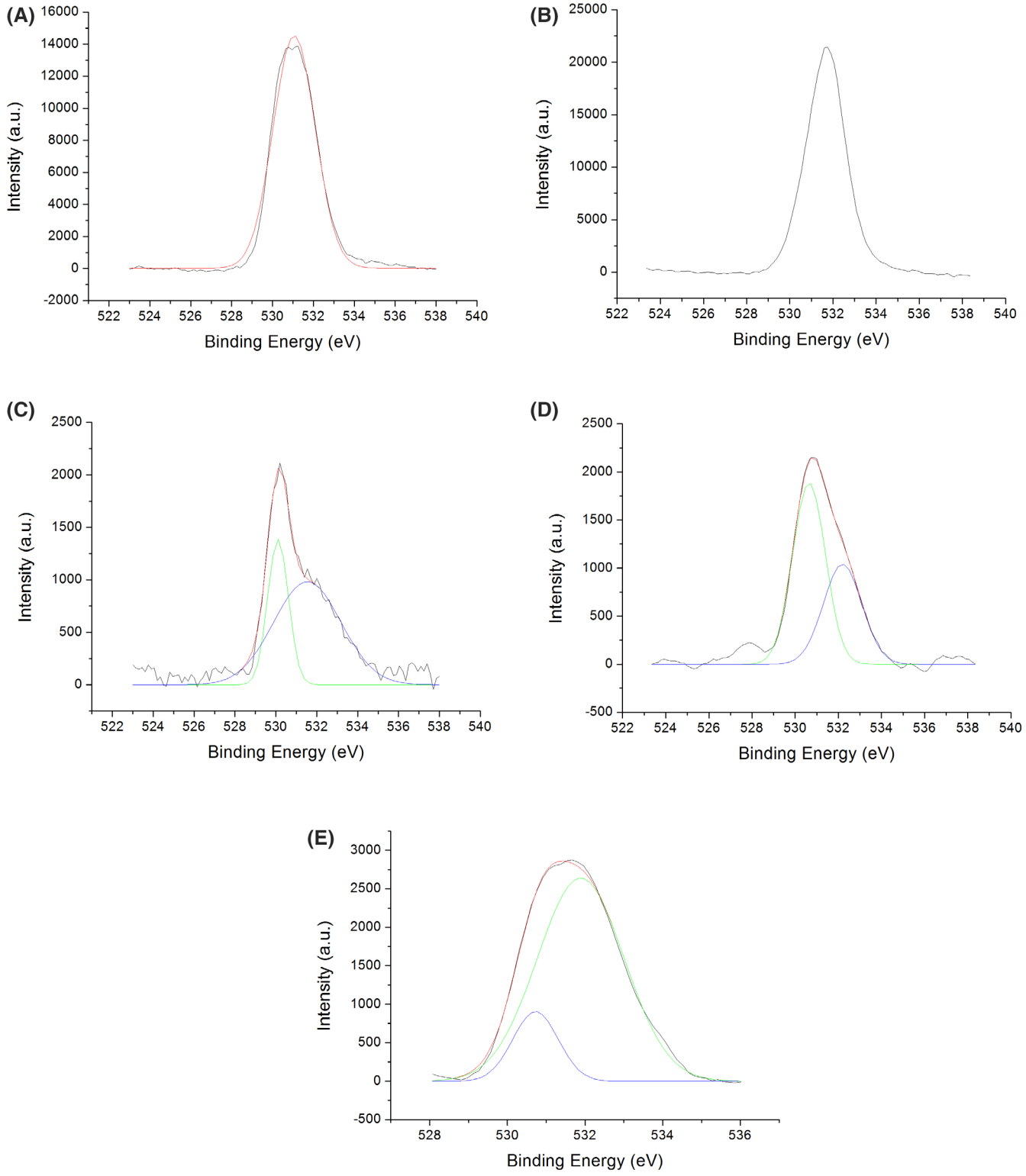

FIGURE 4 O1s spectra of A, G1; B, G3; C, G4; D, G7; and E, G9

around 284.6, 286, and 288 eV for G1 and G3. The relative intensity of sp^3 hybridized carbon are calculated as 73.03 and 68.35 for G1 and G3, so the majority of these structures contain the non-oxygenated ring C atoms in spite of presence of C—O bonds (14.5% and 15.1%) and carboxylate C atoms (12.5% and 16.5%). For G4, G7, and G9 carbon

appears to be in the form of non-oxygenated ring C atoms (sp^3) in very large proportions compared to G1 and G3, and their relative intensities are 91.7, 92.6, and 90.7, respectively (Table 4). These results are much higher than the few-layer graphene prepared using the chemical method.[49] Moreover, the results obtained from XPS are in parallel with SEM-EDX results. The deconvulated O1s peaks of G4, G7, and G9 contain 2 main peaks at around 530 and 531 eV, which corresponds to the form of C═O and C—O. The O 1 second peaks of G1 and G3 are also observed at 531.1 and 531.6 eV, and this was attributed to C—O existence with relative intensity of 100%. The detailed information about the relative intensity of deconvulated C1s and O1s peaks are summarized in Table 4.

Graphene possesses two significant Raman bands, namely, G-band and G'-band located at ca. 1582 cm^{-1} and 2700 cm^{-1}, respectively. G' band is also called 2D-band since its frequency is roughly twice of the D band. Here, D-band located at 1350 cm^{-1} stems from A_{1g} breathing mode of the six-atom rings,[50] and the G-band is related to the E_{2g}.[51,52] Besides, the increase in the 2D/G ratio indicates the decrease in the number of layers while the rise in D/G ratio shows the increase in structural defects of the surface.[51]

TABLE 4 C1s and O1s binding energies of G1, G3, G4, G7, and G9

Catalysts	Species	Binding energy (eV)	Possible chemical state	Relative intensity (%)
G1	C1s	284.6	C—C	73.03
		286.0	C—O	14.51
		288.2	O—C═O	12.45
	O1s	531.1	C—O	100
G3	C1s	284.6	C—C	68.35
		286.4	C—O	15.13
		288.5	O—C═O	16.51
	O1s	531.6	C—O	100
G4	C1s	284.6	C—C	91.72
		286.4	C—O	8.28
	O1s	530.1	C═O	58.6
		531.6	C—O	41.4
G7	C1s	284.6	C—C	92.59
		286.4	C—O	7.42
	O1s	530.5	C═O	54.7
		531.7	C—O	45.3
G9	C1s	284.6	C—C	90.72
		286.4	C—O	9.28
	O1s	530.8	C═O	1107.7
		532.0	C—O	2509.1

Abbreviation: CVD, chemical vapor deposition.

TABLE 5 Peak intensities and ratios obtained from Raman spectrum

Samples	D	G	2D	D/G	2D/G
G1	2.786	58.796	19.821	0.047385	0.33712
G2	9.322	76.933	20.500	0.121165	0.26646
G3	4.59367	13.364	3.516	0.343748	0.263084
G4	1.700	26.040	27.497	0.065266	1.055954
G5	35.004	121.250	72.704	0.288693	0.599621
G6	4.659	24.066	26.058	0.193583	1.082776
G7	15.310	110.550	42.788	0.138489	0.387047
G8	11.890	25.721	19.657	0.462268	0.764239
G9	8.241	20.545	22.588	0.40111	1.09944

Table 5 shows the intensity of D, G, and 2D peaks obtained from the Raman spectra of graphene Figure 5. As can be seen from Table 5, flow rate of hexane and hydrogen was identical for G4 and G5 samples while synthesis duration was 20 minutes longer for G4 than G5. 2D/G ratio of G4 (1.056) was higher than G5 (0.5996). Similar results were obtained for G1 and G2 prepared under the same conditions except for the synthesis duration. From these results, it was determined that the number of layers decreased as the synthesis time increased. The D/G ratios of G1, G2, G4, and G5 were 0.047385, 0.121165, 0.065266, and 0.288693, respectively. G1 and G4 have lower D/G ratio than G2 and G5, indicating that synthesis time was negatively correlated with the number of defects. G4 and G6 were synthesized at the same hexane flow rate and synthesis duration while hydrogen flow rates for G4 and G6 were 25 sscm and 0 sscm. 2D/G ratios for these two samples were calculated as 1.055954 and 1.082776 while the D/G ratios were found as 0.065266 and 0.193583. Accordingly, it was determined that the defect number decreased and the number of layers increased with the decrease of hydrogen flow rate. In addition, when G3 (0.5 sccm), G6 (2.5 sccm), G8 (7.5 sccm), and G9 (5 sccm) samples prepared at different rates of hexane flow were analyzed, it was observed that the number of layers decreased with increasing flow rate.

3.2 | Electrochemical measurements

Electrocatalytic activities of obtained few-layer graphene/ITO electrodes were examined by CV in 1 M KOH + 0.5 M glucose solution. Figure 6A shows GOR measurements among ITO-G9 electrodes at a potential range of −0.6~0.4 V at a scan

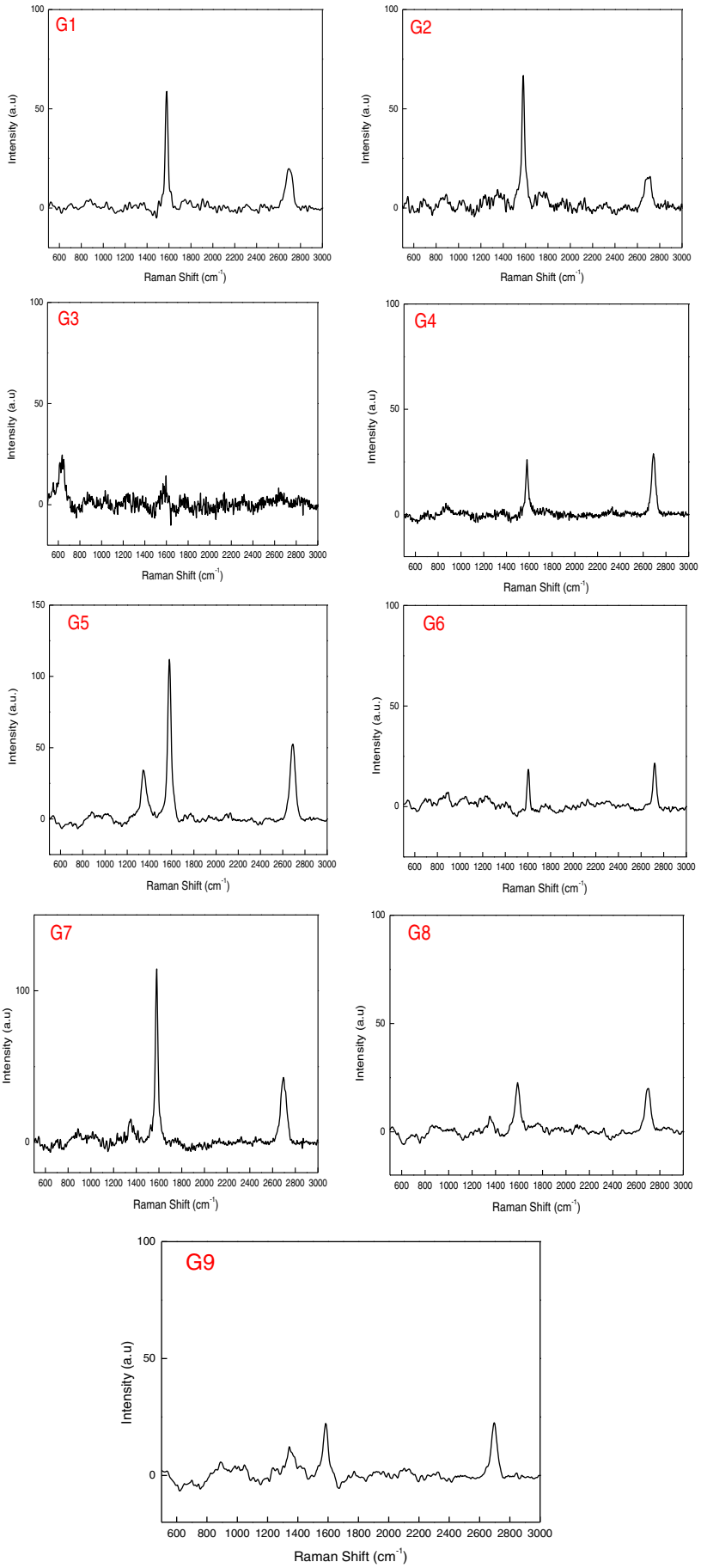

FIGURE 5 Raman spectra of G1, G2, G3, G4, G5, G6, G7, G8, and G9

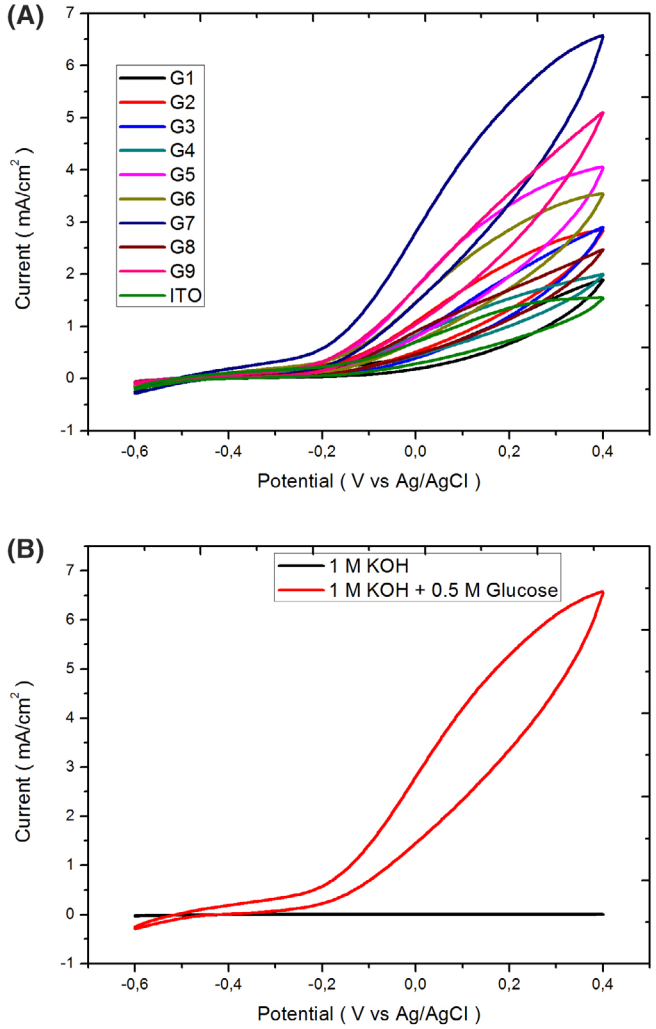

FIGURE 6 Cyclic voltammetry obtained in A, among ITO-G9 electrodes in 1 M KOH + 0.5 M glucose solution; B, the G7 electrodes in 1 M KOH and 1 M KOH + 0.5 M glucose solution; scan rate: 50 mV s^{-1}. ITO, indium tin oxide

rate of 50 mV s^{-1}. The specific activity, peak potential (E_p), and onset potential (E_{on}) of among these electrodes are given in Table 6. As shown in Table 6, the G7/ITO electrode exhibited better activity than ITO electrode about 4.2 times and other electrodes. Besides, the G7/ITO electrode was approximately exhibited better activity than the literature studies given in Table 1. During forward scanning, glucose to form an adsorbed intermediate for all electrodes. The decrease in current at potentials more positive with respect to the peak potential could be due to the formation which rivals for surface adsorption sites with glucose and in turn hinders the GOR as well. During the reverse scan, oxidation of glucose occurs, in the potential region in which the surface oxides are reduced.[26] Figure 6B indicates the CV of G7/ITO electrode in 1 M KOH and 1 M KOH + 0.5 M glucose solution. As seen in Figure 6B was obtained for glucose electrooxidation a clear oxidation peak in the G7/ITO electrode.

The stability and response of these electrodes in 1 M KOH and 0.5 M glucose solution was obtained with 0.2, 0.3, and 0.4 V at 1000 seconds CA measurement. Figure 7A shows the CA curves of the electrodes. Among these electrodes, the G7/ITO electrode was showed better activity and stability than the other electrodes. In addition, G7/ITO electrode was carried out with good activity in CA results as with CV results. Figure 7B shows the CA measurements of the G7/ITO electrode at different potentials. As shown in Figure 6B, the best activity of 0.4 V was obtained. Moreover, Figure 7C displays the current values of the electrodes after 1000 seconds. Here, G7/ITO electrode was approximately performed 1.5 times activity from the ITO electrode and it was obtained activity better than the other electrodes.

Nyquist plots of few-layer graphene/ITO electrodes obtained with EIS results were used to show the best resistance towards GOR. Nyquist plots are generally known to be semicircular in structure and the smaller the diameter, the higher the electrocatalytic resistance. Furthermore, these semicircle diameters of Nyquist plots are related to charge transfer resistance (Rct) associated with the electrocatalytic activity of few-layer graphene/ITO electrodes.[18,53,54] EIS measurements of graphene/ITO electrodes and Nyquist plots for GOR are given in Figure 8A. As shown in Figure 8A, the Rct resistances of the few-layer graphene/ITO electrodes were obtained in the order of G7 > G9 > G8 > G1 > G6 > G2 > G4 > G3 > G5 > ITO for GOR, respectively. As a result, G7/ITO electrode was shown in the best GOR activity as with CV and CA results. Figure 8B, EIS measurements of G7/ITO electrode are given at different volts and the best GOR activity is obtained in 0.4 V.

TABLE 6 Glucose electrooxidation specific activity, E_p, and E_{on} values for among ITO-G9 electrodes

Electrodes	Specific activity (mA/cm^2)	E_p (V)	E_{on} (V)
ITO	1.56	0.4	−0.23
G1	1.90	0.4	−0.39
G2	2.85	0.4	−0.38
G3	2.90	0.4	−0.33
G4	1.99	0.4	−0.25
G5	4.10	0.4	−0.24
G6	3.54	0.4	−0.23
G7	6.58	0.4	−0.24
G8	2.47	0.4	−0.25
G9	5.09	0.4	−0.24

Abbreviation: ITO, indium tin oxide.

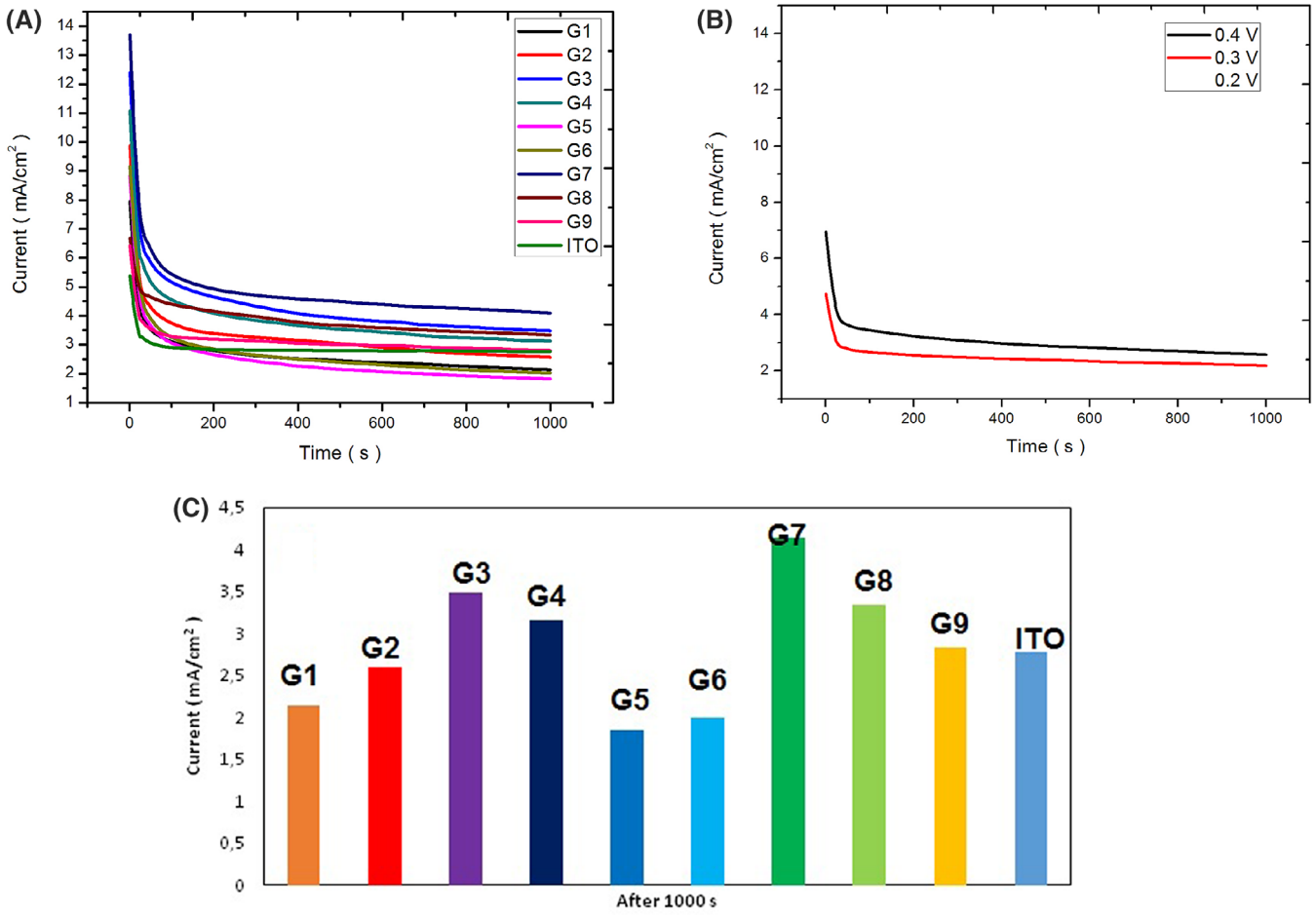

FIGURE 7 Glucose electrooxidation of few-layer graphene/ITO electrodes obtained A, chronoamperometry curves of among ITO-G9 electrodes at 0.4 V and 1000 seconds; B, chronoamperometry curves of G7/ITO electrode at different volts; C, the current after 1000 seconds. ITO, indium tin oxide

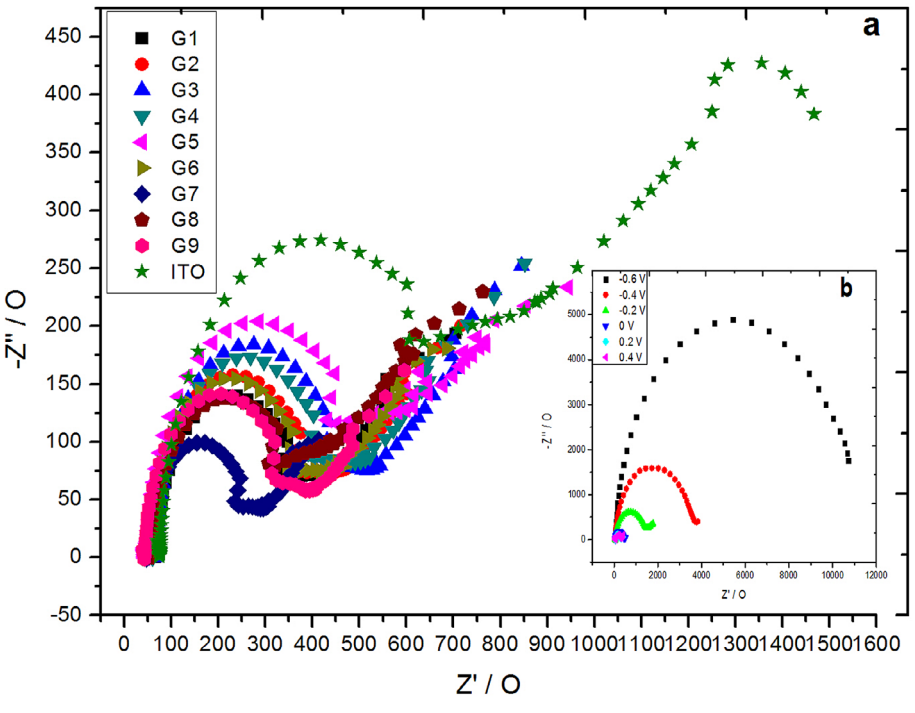

FIGURE 8 Nyquist plots EIS of few-layer graphene/ITO electrodes obtained A, among ITO-G9 electrodes 0.4 V; B, G7 electrode at different volts: 1 M KOH + 0.5 M glucose. EIS, electrochemical impedance spectroscopy; ITO, indium tin oxide

4 | CONCLUSIONS

In this study, few-layer graphene was coated on Cu foils via CVD method by varying synthesis parameters as hexane and hydrogen flow rate and deposition time to optimize synthesis conditions through GOR. After few-layer graphene produced on Cu, the few-layer graphene was coated onto the ITO electrode. The graphene network was clearly visible from SEM images. The deconvulated XPS spectra indicated that carbon appeared in form of the non-oxygenated ring C atoms for G1, G3, G4, G7, and G9. The few-layer graphene structure was confirmed by Raman analysis. Among the graphene/ITO electrodes, G7/ITO electrode exhibited the best electrochemical activity towards GOR. The GOR specific activity of G7/ITO electrode was obtained as 6.58 mA cm^{-2} in alkaline environment. This value is better than the ones measured for other electrodes. The results show that G7/ITO electrode exhibited approximately better specific activity than the literature studies.

ACKNOWLEDGMENTS

Authors would like to thank for the financial support for The Scientific and Technological Research Council of Turkey TUBITAK project (project no: 116M004).

ORCID

Berdan Ulas https://orcid.org/0000-0003-0650-0316
Hilal Demir Kivrak https://orcid.org/0000-0001-8001-7854

REFERENCES

1. Ulas B, Caglar A, Kivrak A, Kivrak H. Atomic molar ratio optimization of carbon nanotube supported PdAuCo catalysts for ethylene glycol and methanol electrooxidation in alkaline media. *Chem Pap*. 2018;73(2):425-434.
2. Ulas B, Caglar A, Sahin O, Kivrak H. Composition dependent activity of PdAgNi alloy catalysts for formic acid electrooxidation. *J Colloid Interface Sci*. 2018;532:47-57.
3. Çağlar A, Aldemir A, Kivrak H. Alcohol electrooxidation study on carbon nanotube supported monometallic, Pt, Bi, and Ru catalysts. *Fullerenes, Nanotubes and Carbon Nanostructures*. 2018;26(12):863-870.
4. Bulut A, Yurderi M, Karatas Y, et al. Pd-MnOx nanoparticles dispersed on amine-grafted silica: highly efficient nanocatalyst for hydrogen production from additive-free dehydrogenation of formic acid under mild conditions. *Appl Catal Environ*. 2015;164:324-333.
5. Kivrak H, Atbas D, Alal O, et al. A complementary study on novel PdAuCo catalysts: synthesis, characterization, direct formic acid fuel cell application, and exergy analysis. *Int J Hydrogen Energy*. 2018;43:21886-21898.
6. Sharma R, Andersen SM. An opinion on catalyst degradation mechanisms during catalyst support focused accelerated stress test (AST) for proton exchange membrane fuel cells (PEMFCs). *Appl Catal Environ*. 2018;239:636-643.
7. Bulut A, Yurderi M, Karatas Y, et al. MnOx-promoted PdAg alloy nanoparticles for the additive-free dehydrogenation of formic acid at room temperature. *ACS Catal*. 2015;5:6099-6110.
8. Karatas Y, Bulut A, Yurderi M, et al. PdAu-MnO_x nanoparticles supported on amine-functionalized SiO_2 for the room temperature dehydrogenation of formic acid in the absence of additives. *Appl Catal Environ*. 2016;180:586-595.
9. Sahin O, Kivrak H. A comparative study of electrochemical methods on Pt–Ru DMFC anode catalysts: the effect of Ru addition. *Int J Hydrogen Energy*. 2013;38:901-909.
10. Kivrak HD. The effect of temperature and concentration for methanol electrooxidation on Pt-Ru catalyst synthesized by microwave assisted route. *Turk J Chem*. 2015;39:563-575.
11. Kivrak H, Can M, Duru H, Sahin O. Methanol electrooxidation study on mesoporous silica supported Pt–Co direct methanol fuel cell anode. *International Journal of Chemical Reactor Engineering*. China: Degruyter; 2014;12(1):369. https://doi.org/10.1515/ijcre-2014-0051
12. Sahin O, Duzenli D, Kivrak H. An ethanol electrooxidation study on carbon-supported Pt-Ru nanoparticles for direct ethanol fuel cells. *Energy Sources, Part A*. 2016;38:628-634.
13. Kivrak H, Demir NC, Şahin Ö. Electrocatalytic Properties Of Nanostructured Multimetallic Pt-Sn-Cs/C and Pt-M/C (M= Ag, Ca, Cd, Cs, Cu, Fe, Ir, Mg, Pd, Sn, Zr) Direct Ethanol Fuel Cell Catalysts. *Selcuk University Journal of Engineering, Science & Technology/Selçuk Üniversitesi Mühendislik, Bilim ve Teknoloji Dergisi*. 2013;1:19-28.
14. Guo Z, Li Y, Guo H. Effect of light/dark regimens on hydrogen production by Tetraselmis subcordiformis coupled with an alkaline fuel cell system. *Appl Biochem Biotechnol*. 2017;183:1295-1303.
15. Caglar A, Sahan T, Cogenli MS, Yurtcan AB, Aktas N, Kivrak H. A novel central composite design based response surface methodology optimization study for the synthesis of Pd/CNT direct formic acid fuel cell anode catalyst. *Int J Hydrogen Energy*. 2018;43:11002-11011.
16. Senthilkumar N, Gnana kumar G, Manthiram A. 3D hierarchical Core–Shell nanostructured arrays on carbon fibers as catalysts for direct urea fuel cells. *Adv Energy Mater*. 2018;8:1702207.
17. Raj kumar T, Gnana kumar G, Manthiram A. Biomass-derived 3D carbon aerogel with carbon Shell-confined binary metallic nanoparticles in CNTs as an efficient Electrocatalyst for microfluidic direct ethylene glycol fuel cells. *Adv Energy Mater*. 2019;9:1803238. https://doi.org/10.1002/aenm.201803238
18. Zhiani M, Abedini A, Majidi S. Comparison of electro-catalytic activity of Fe-Ni-co/C and Pd/C nanoparticles for glucose electro-oxidation in alkaline half-cell and direct glucose fuel cell. *Electrocatalysis*. 2018;9:735-743.
19. Yan L, Brouzgou A, Meng Y, Xiao M, Tsiakaras P, Song S. Efficient and poison-tolerant PdxAuy/C binary electrocatalysts for glucose electrooxidation in alkaline medium. *Appl Catal Environ*. 2014;150-151:268-274.
20. Chai D, Wang W, Wang F, Kang Y, Yang Y, Lei Z. A facile precipitation procedure for synthesis of binary Sn-co oxide promoting Pd catalyst towards glucose electrooxidation. *Electrochim Acta*. 2016;189:295-302.
21. Hsieh C-T, Chen Y-F, Yu P-Y. Deposition of binary Pd–Rh catalysts on nanostructured carbon supports for non-enzymatic glucose oxidation. *Int J Hydrogen Energy*. 2015;40:14857-14865.

22. Ramachandran K, Raj kumar T, Babu KJ, Gnana kumar G. Ni-Co bimetal nanowires filled multiwalled carbon nanotubes for the highly sensitive and selective non-enzymatic glucose sensor applications. *Sci Rep*. 2016;6:36583.
23. Siva G, Aziz MA, Gnana kumar G. Engineered tubular Nanocomposite Electrocatalysts based on CuS for high-performance, durable glucose fuel cells and their stack. *ACS Sustainable Chem Eng*. 2018;6:5929-5939.
24. Hsieh C-T, Lin W-H, Chen Y-F, Tzou D-Y, Chen P-Q, Juang R-S. Microwave synthesis of copper catalysts onto reduced graphene oxide sheets for non-enzymatic glucose oxidation. *J Taiwan Inst Chem Eng*. 2017;71:77-83.
25. Brouzgou A, Song S, Tsiakaras P. Carbon-supported PdSn and Pd3Sn2 anodes for glucose electrooxidation in alkaline media. *Appl Catal Environ*. 2014;158-159:209-216.
26. Brouzgou A, Yan LL, Song SQ, Tsiakaras P. Glucose electrooxidation over PdxRh/C electrocatalysts in alkaline medium. *Appl Catal Environ*. 2014;147:481-489.
27. Li L, Scott K, Yu EH. A direct glucose alkaline fuel cell using MnO_2–carbon nanocomposite supported gold catalyst for anode glucose oxidation. *J Power Sources*. 2013;221:1-5.
28. Rafaïdeen T, Baranton S, Coutanceau C. Highly efficient and selective electrooxidation of glucose and xylose in alkaline medium at carbon supported alloyed PdAu nanocatalysts. *Appl Catal Environ*. 2019;243:641-656.
29. Gao M, Liu X, Irfan M, Shi J, Wang X, Zhang P. Nickle-cobalt composite catalyst-modified activated carbon anode for direct glucose alkaline fuel cell. *Int J Hydrogen Energy*. 2018;43:1805-1815.
30. Chen C-C, Lin C-L, Chen L-C. A binary palladium–bismuth nanocatalyst with high activity and stability for alkaline glucose electrooxidation. *J Power Sources*. 2015;287:323-333.
31. Song S, Wang K, Yan L, et al. Ceria promoted Pd/C catalysts for glucose electrooxidation in alkaline media. *Appl Catal Environ*. 2015;176–177:233-239.
32. Basu D, Basu S. Performance studies of Pd–Pt and Pt–Pd–Au catalyst for electro-oxidation of glucose in direct glucose fuel cell. *Int J Hydrogen Energy*. 2012;37:4678-4684.
33. Bollella P, Fusco G, Tortolini C, et al. Beyond graphene: electrochemical sensors and biosensors for biomarkers detection. *Biosens Bioelectron*. 2017;89, Part 1:152-166.
34. Geng D, Bo X, Guo L. Ni-doped molybdenum disulfide nanoparticles anchored on reduced graphene oxide as novel electroactive material for a non-enzymatic glucose sensor. *Sens Actuators B*. 2017;244:131-141.
35. Wang C-H, Yang C-H, Chang J-K. High-selectivity electrochemical non-enzymatic sensors based on graphene/Pd nanocomposites functionalized with designated ionic liquids. *Biosens Bioelectron*. 2017;89, Part 1:483-488.
36. Tajabadi MT, Sookhakian M, Zalnezhad E, et al. Electrodeposition of flower-like platinum on electrophoretically grown nitrogen-doped graphene as a highly sensitive electrochemical non-enzymatic biosensor for hydrogen peroxide detection. *Appl Surf Sci*. 2016;386:418-426.
37. Tan YY, Jayawardena KDGI, Adikaari AADT, et al. Photothermal chemical vapor deposition growth of graphene. *Carbon*. 2012;50:668-673.
38. Yao Y, Wong C-p. Monolayer graphene growth using additional etching process in atmospheric pressure chemical vapor deposition. *Carbon*. 2012;50:5203-5209.
39. Liu R, Chi Y, Fang L, Tang Z, Yi X. Synthesis of carbon nanowall by plasma-enhanced chemical vapor deposition method. *J Nanosci Nanotechnol*. 2014;14:1647-1657.
40. Seo J, Lee J, Jang AR, et al. Study of cooling rate on the growth of Graphene via chemical vapor deposition. *Chem Mater*. 2017;29:4202-4208.
41. Chen K, Chen L, Chen Y, Bai H, Li L. Three-dimensional porous graphene-based composite materials: electrochemical synthesis and application. *J Mater Chem*. 2012;22:20968-20976.
42. Lee W, Kihm KD, Kim HG, et al. In-plane thermal conductivity of polycrystalline chemical vapor deposition graphene with controlled grain sizes. *Nano Lett*. 2017;17:2361-2366.
43. Ghaemi F, Abdullah LC, Tahir PM, Yunus R. Synthesis of different layers of graphene on stainless steel using the CVD method. *Nanoscale Res Lett*. 2016;11:506.
44. Wimalananda MDSL, Kim J-K, Lee J-M. Rapid synthesis of a continuous graphene film by chemical vapor deposition on Cu foil with the various morphological conditions modified by Ar plasma. *Carbon*. 2017;120:176-184.
45. Murdock AT, van Engers CD, Britton J, et al. Targeted removal of copper foil surface impurities for improved synthesis of CVD graphene. *Carbon*. 2017;122:207-216.
46. Kong J, Cassell AM, Dai H. Chemical vapor deposition of hexane for single-walled carbon nanotubes. *Chem Phys Lett*. 1998;292:567-574.
47. Yu J, Li J, Zhang W, Chang H. Synthesis of high quality two-dimensional materials via chemical vapor deposition. *Chem Sci*. 2015;6:6705-6716.
48. Li X, Cai W, An J, et al. Large-area synthesis of high-quality and uniform graphene films on copper foils. *Science*. 2009;324:1312-1314.
49. Wu Y, Wang B, Ma Y, et al. Efficient and large-scale synthesis of few-layered graphene using an arc-discharge method and conductivity studies of the resulting films. *Nano Res*. 2010;3:661-669.
50. Li X, Liu Y, Zeng Z, Wang P, Fang Y, Zhang L. Investigation on tip enhanced Raman spectra of graphene. *Spectrochim Acta A Mol Biomol Spectrosc*. 2018;190:378-382.
51. Rogalski J, Braun K, Horneber A, et al. STM tip-enhanced Raman spectroscopy and the investigation of doped graphene. *Vib Spectrosc*. 2017;91:128-135.
52. Calizo I, Ghosh S, Bao W, Miao F, Ning Lau C, Balandin AA. Raman nanometrology of graphene: temperature and substrate effects. *Solid State Commun*. 2009;149:1132-1135.
53. Yang Y, Jin L, Liu B, Kerns P, He J. Direct growth of ultrasmall bimetallic AuPd nanoparticles supported on nitrided carbon towards ethanol electrooxidation. *Electrochim Acta*. 2018;269:441-451.
54. Wang F, Yu H, Tian Z, Xue H, Feng L. Active sites contribution from nanostructured interface of palladium and cerium oxide with enhanced catalytic performance for alcohols oxidation in alkaline solution. *J Energy Chem*. 2018;27:395-403.

How to cite this article: Caglar A, Ulas B, Sahin O, Demir Kivrak H. Few-layer graphene coated on indium tin oxide electrodes prepared by chemical vapor deposition and their enhanced glucose electrooxidation activity. *Energy Storage*. 2019;1:e73. https://doi.org/10.1002/est2.73